Available online at www.sciencedirect.com

ScienceDirect

Advances in Space Research 72 (2023) 1583–1592

ADVANCES IN SPACE RESEARCH (a COSPAR publication)

www.elsevier.com/locate/asr

Adaptive fault-tolerant control for spacecraft formation under external disturbances with guaranteed performance

Yuedong Wu [a,b], Wei Wang [a,*], Hongxu Zhu [a], Shufan Wu [a,*], Christopher J. Damaren [b]

[a] School of Aeronautics and Astronautics, Shanghai Jiaotong University, Shanghai 200240, China
[b] Institute for Aerospace Studies, University of Toronto, Ontario M3H 5T6, Canada

Received 29 November 2022; received in revised form 4 May 2023; accepted 4 May 2023
Available online 10 May 2023

Abstract

This paper investigates an adaptive fault-tolerant control problem for spacecraft formation flying (SFF) with actuator faults, external disturbances, and unknown inertial uncertainties. First, fault factors are introduced to describe the SFF orbit model with consideration of actuator bias faults and loss of actuator effectiveness. Then, an adaptive fault-tolerant controller is proposed by incorporating prescribed performance function, improved terminal sliding mode control and the proposed adaptive law. Finally, rigorous theoretical analysis ensures the uniformly ultimately bounded stability of the system through Lyapunov theory and simulation verifies the proposed algorithm.

Keywords: Fault-tolerant control; Spacecraft formation flying; Sliding-mode control; Prescribed performance

1. Introduction

With the development of space technology, space missions are increasingly diversified and autonomous (Wen et al., 2020; Lian et al., 2021). The emerging space missions represented by on-orbit service and maintenance, formation flying and deep space exploration are increasing (Fraser and Ulrich, 2021). The spacecraft formation flying (SFF) system composed of multiple spacecraft has received continuous attention and investment from various space powers due to its robustness, flexibility, low cost and reliability (Mauro et al., 2018; Liu and Zhang, 2018). The SFF system is also used in on-orbit distributed sensing, earth observation, stereo imaging, terrain mapping, etc (Zhuang et al., 2021b). Laser Interferometer Space Antenna (LISA) led by ESA, and TianQin and Taiji projects proposed by China all use SFF system to detect gravitational wave in space (Xie et al., 2023; Amaro-Seoane et al., 2017; Luo et al., 2016; Hu and Wu, 2017).

In real spacecraft missions, the SFF system faces enormous challenges due to the harsh space environment and other factors. Although spacecraft are thoroughly tested before launching, many spacecraft come across faults and failures (Harland and Lorenz, 2005; Clark, 2016; Hasan et al., 2022). Through the analysis of 872 faults from 1960 to 2012, two reports concluded that the fault rate of Attitude and Orbit Control System (AOCS) was the highest (Tan et al., 2011; Ji et al., 2019). Therefore, it is significant for the spacecraft to have the ability to handle faults autonomously. Since the 1980s, scholars began to study Fault-Tolerant Control (FTC) (Yin et al., 2016). Passive Fault-tolerant control has attracted extensive attention in the space engineering and academic communities due to its advantages of not requiring fault online information

* Corresponding authors.
E-mail addresses: wuyuedong@sjtu.edu.cn (Y. Wu), wangwei215661@sjtu.edu.cn (W. Wang), hcwsdxuxu@163.com (H. Zhu), shufan.wu@sjtu.edu.cn (S. Wu), chris.damaren@utoronto.ca (C.J. Damaren).

https://doi.org/10.1016/j.asr.2023.05.008
0273-1177/

and being able to handle multiple types of faults simultaneously (Han et al., 2015; Zhu and Guo, 2018; Hu et al., 2019; Yi et al., 2019; Wang et al., 2020; Wang et al., 2021; Yue et al., 2020). In Ref. (Zhang et al., 2021), a new fault-tolerant control scheme based on neural networks and event-triggered control was proposed. In Ref. (Cao et al., 2022), an adaptive learning observer design method without perturbation upper limit was proposed, which can accurately and quickly estimate attitude angular velocity and reconstruct actuator faults. On the other hand, in real SFF system missions, external disturbances and model uncertainties are inevitable. To solve these problems, many effective controllers have been proposed, such as robust control (Luo et al., 2005; Liu et al., 2017), sliding mode control (Hu, 2008; Di et al., 2021), active disturbance rejection control (Bai et al., 2018), disturbance observer based control (Zhu et al., 2020) and so on. Terminal Sliding Mode Control (TSMC) has attracted the attention of many scholars due to its strong robustness and finite-time convergence (Lu and Xia, 2013; Zhang et al., 2018; Guo et al., 2019; Zhang et al., 2020; Zhang and Li, 2022; Artitthang et al., 2023). However, the aforementioned proposed controllers only analyze the system stability and steady-state behavior, without considering the transient performance metrics. To constrain system transient response, prescribed performance control (PPC) was creatively proposed by Bechlioulis and Rovithakis (Bechlioulis and Rovithakis, 2008). In recent years, PPC is widely used in SFF system (Wei et al., 2021; Wang et al., 2022; Li et al., 2018; Mehdifar et al., 2020; Liu et al., 2023). In Ref. (Zhuang et al., 2021a), according to the PPC structure, the fixed-time control problem of SFF system reconstruction under input saturation was proposed. In Ref. (Yin et al., 2022), based on the PPC structure, the fixed-time cooperative FTC in heterogeneous satellite formation systems was studied. In Ref. (Wei et al., 2022), an adaptive leader-following formation tracking control method was proposed for the SFF system considering external disturbances, directed communication topology, limited sensing ranges, and formation safety.

Nevertheless, to the author's best knowledge, although many factors have been considered in the above literature, few studies have considered adaptive fault-tolerant, transient performance metrics, robustness and fast convergence for the SFF system at the same time. In gravitational wave detection missions, the gravitational wave signal is tiny, and the space environment is complicated, which puts forward more complicated requirements for the SFF controller (Gong et al., 2021). Therefore, it is critical to consider the above factors simultaneously. Specifically, in this paper, an adaptive fault-tolerant controller is proposed. Firstly, the SFF system model simultaneously includes actuator faults, external disturbances and unknown inertial uncertainties, which can better reflect real space missions. Besides a novel integrated control scheme combining the improved TSMC, the proposed adaptive law and PPC are put forward for the SFF system. Such a control scheme can achieve the formation reconfiguration with prescribed behavioral metrics, despite the presence of actuator faults, external disturbances, and unknown inertial uncertainties. Finally, the stability of the proposed control method is proved theoretically via the Lyapunov function, and simulation proves the proposed control algorithm.

The organization of the rest paper is as follows: Section 2 states the relative dynamics of the SFF system, actuator fault model and graph theory. Section 3 states the design and stability analysis of the adaptive fault-tolerant controller based on PPC. Section 4 states numerical simulation to validate the correctness of the proposed control algorithm. Finally, Section 5 concludes this paper.

2. Problem formulations and preliminaries

In this section, some basic concepts of controlled objects are provided, including relative dynamics, acuator fault model, graph theory and so on.

2.1. Relative dynamics description

To describe SFF system formed by N spacecraft, a virtual reference spacecraft is proposed as a standard to provide relative position and velocity for the SFF system. As Fig. 1. shows, F_I represents the Earth Centered Inertial (ECI) frame. The origin of F_I is located at the center mass of the Earth. The X_I axis points to the Vernal Equinox, the Z_I axis points to the Earth's north pole, and the Y_I axis meets the third axis of the right-hand frame. F_C represents the Local Vertical Local Horizontal (LVLH) frame. The origin of F_C is located at the center mass of the reference spacecraft, and the three coordinate axes correspond to the three inertia principal axes of the reference spacecraft respectively. $\boldsymbol{r}_c \in \mathbb{R}^3$ and $\boldsymbol{r}_i \in \mathbb{R}^3$ represent the position vectors from the Earth center to reference spacecraft and i-th spacecraft respectively. $\boldsymbol{p}_i = [x_i,\ y_i,\ z_i]^{\mathrm{T}}$ denotes the relative position vector for the i-th spacecraft in the F_C frame, where $i = 1, 2 \ldots N$ is the total number of spacecraft. $\boldsymbol{v}_i$ is the relative velocity vector. Then, the relative dynamics of the i-th spacecraft with respect to F_C can be written as:

$$\dot{\boldsymbol{p}}_i = \boldsymbol{v}_i \tag{1}$$

$$m_i \dot{\boldsymbol{v}}_i = \boldsymbol{C}_i \boldsymbol{v}_i + \boldsymbol{D}_i \boldsymbol{p}_i + \boldsymbol{n}_i + \boldsymbol{d}_i + \boldsymbol{u}_i \tag{2}$$

where m_i is the mass of the i-th spacecraft, $\boldsymbol{d}_i = \left[d_{ix},\ d_{iy},\ d_{iz}\right]^{\mathrm{T}}$ is the external disturbances vector (including J_2 perturbation and other disturbances) and $\boldsymbol{u}_i = \left[u_{ix},\ u_{iy},\ u_{iz}\right]^{\mathrm{T}}$ is the actual control input vector. The other matrices are

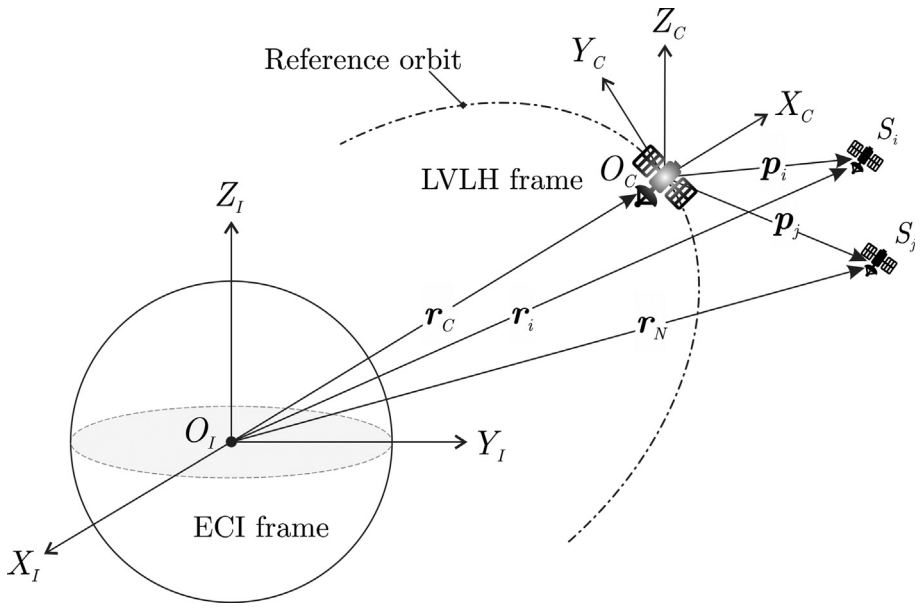

Fig. 1. Schematic representation of coordinate frames.

$$\boldsymbol{C}_i = 2m_i\dot{\theta}\begin{bmatrix} 0 & 1 & 0 \\ -1 & 0 & 0 \\ 0 & 0 & 0 \end{bmatrix},$$

$$\boldsymbol{D}_i = m_i\begin{bmatrix} \dot{\theta}^2 - \frac{\mu}{r_i^3} & \ddot{\theta} & 0 \\ -\ddot{\theta} & \dot{\theta}^2 - \frac{\mu}{r_i^3} & 0 \\ 0 & 0 & -\frac{\mu}{r_i^3} \end{bmatrix}, \tag{3}$$

$$\boldsymbol{n}_i = \mu m_i\begin{bmatrix} -\frac{r_c}{r_i^3} + \frac{1}{r_c^2} \\ 0 \\ 0 \end{bmatrix}$$

where $\dot{\theta}$ is the true anomaly of the reference spacecraft, μ is the gravitational constant of the earth, $r_i = \sqrt{(x_i + r_c)^2 + y_i^2 + z_i^2}$, and $r_c = \|\boldsymbol{r}_c\|$.

2.2. Acuator fault model

Eq. (1) and Eq. (2) provide the relative dynamics model for the i-th spacecraft. However, the space environment is very complicated. The spacecraft may suffer from huge temperature changes and various space radiation during operation, which will lead to actuator faults. Summarize the modeling of the fault, then the actual output with actuator fault can be modeled as

$$\tilde{\boldsymbol{u}}_i = \boldsymbol{H}_i\boldsymbol{u}_i + \boldsymbol{\epsilon}_i \tag{4}$$

where $\boldsymbol{H}_i \triangleq \mathrm{diag}(h_{ix}, h_{iy}, h_{iz})$ stands for the healthy indicator matrix, $h_i (0 \leqslant h_i \leqslant 1)$ is the loss of actuator effectiveness, and $\boldsymbol{\epsilon}_i \triangleq [\epsilon_{ix}, \epsilon_{iy}, \epsilon_{iz}]^{\mathrm{T}}$ reflects the actuator bias faults. Without loss of generality, the effectiveness loss and bias fault should be considered for the SFF system. Eq. (2) can be slightly modified according to Eq. (4). Then, the SFF relative dynamics model including actuator faults can be modeled as

$$m_i\dot{\boldsymbol{v}}_i = \boldsymbol{C}_i\boldsymbol{v}_i + \boldsymbol{D}_i\boldsymbol{p}_i + \boldsymbol{n}_i + \boldsymbol{d}_i + \boldsymbol{\epsilon}_i + \boldsymbol{H}_i\boldsymbol{u}_i \tag{5}$$

where $\boldsymbol{H}_i \in (\boldsymbol{O}_3, \boldsymbol{I}_3)$, $\boldsymbol{O}_3 \in \mathbb{R}^{3\times3}$ is the zero matrix, $\boldsymbol{I}_3 \in \mathbb{R}^{3\times3}$ is the identity matrix, and $\boldsymbol{\epsilon}_i \neq \boldsymbol{0}_3$.

Let $\boldsymbol{p}_{id} \triangleq [p_{idx}, p_{idy}, p_{idz}]^{\mathrm{T}}$ denote the desired position of the i-th spacecraft with respect to F_c. The corresponding positional error can be expressed as $\boldsymbol{e}_i = \boldsymbol{p}_i - \boldsymbol{p}_{id}$. Then, based on Eq. (5), the positional error dynamics including actuator faults can be expressed as

$$m_i\ddot{\boldsymbol{e}}_i = \boldsymbol{C}_i\dot{\boldsymbol{e}}_i + \boldsymbol{D}_i\boldsymbol{e}_i + \boldsymbol{g}_i + \boldsymbol{d}_i + \boldsymbol{\epsilon}_i + \boldsymbol{H}_i\boldsymbol{u}_i \tag{6}$$

where $\boldsymbol{g}_i = \boldsymbol{C}_i\dot{\boldsymbol{p}}_{id} + \boldsymbol{D}_i\boldsymbol{p}_{id} + \boldsymbol{n}_i - m_i\ddot{\boldsymbol{p}}_{id}$.

2.3. Graph theory

In the topology model of the SFF system, each spacecraft is represented by a vertex, and the information flow between vertices is denoted by a weighted edge Wang et al. (2017). The weighted undirected graph is denoted as $\mathcal{G} = (\mathcal{V}, \mathcal{E}, \mathcal{A})$, where $\mathcal{V} \triangleq \{v_1, \ldots, v_N\}$ is a finite nonempty vertex set. $\mathcal{E} \triangleq \{(v_1, v_2), \ldots, (v_{N-1}, v_N)\} \subseteq \mathcal{V} \times \mathcal{V}$ is the set of edges. $\mathcal{A} = [a_{ij}] \in \mathbb{R}^{\mathrm{N}\times\mathrm{N}}$ is the weighted adjacency matrix whose generic entry is $a_{ij} > 0, \forall (v_j, v_i) \in \mathcal{E}$ with $i \neq j$, and $a_{ii} = 0$. v_i represents the i-th spacecraft. The Laplacian matrix $\mathcal{L} = [l_{ij}] \in \mathbb{R}^{\mathrm{N}\times\mathrm{N}}$ is defined as $\mathcal{L} \triangleq \mathcal{D} - \mathcal{A}$, where $\mathcal{D} = \mathrm{diag}[\mathfrak{d}_1, \ldots, \mathfrak{d}_N] \in \mathbb{R}^{\mathrm{N}\times\mathrm{N}}$ is the in-degree matrix and $\mathfrak{d}_i = \sum_{j=1}^{N} a_{ij}, \forall i \neq j$. N is the total number of the spacecraft in the SFF system.

In this work, undirected graph theory is used to describe the communication topology. An undirected graph has the following characteristics:

(1) An edge $(\upsilon_i, \upsilon_j) \in \mathcal{E}$ means that a bidirectional path and the mutual transmission of information between vertex υ_i and υ_j.

(2) The weighted adjacency matrix $\mathcal{A}$ is sysmmetric.

(3) $\mathcal{L}$ is symmetric positive semi-definite and satisfies $l_{ij} < 0$ and $\sum_{j=1}^{N} l_{ij} = 0, \forall i \neq j$.

3. Controller design

In this section, the error is converted firstly based on the PPC structure, then the controller is proposed for the converted state by using improved TSMC and a novel adaptive law, and finally the stability is proved.

Before implementing the controller design procedure, according to the definitions of undirected graph $\mathcal{G}$ and Laplace matrix $\mathcal{L}$, global formation tracking error of the i-th spacecraft is expressed as

$$\boldsymbol{\Delta}_i = \boldsymbol{e}_i + \sum_{j \in N_i} l_{ij} \boldsymbol{e}_j \tag{7}$$

where $\boldsymbol{\Delta}_i = \left[\Delta_{ix}, \Delta_{iy}, \Delta_{iz}\right]^{\mathrm{T}}$, l_{ij} is the element of $\mathcal{L}$. Taking the second derivative of Eq. (7), one can obtain

$$\begin{aligned} \boldsymbol{\Delta}_i = & \frac{1}{m_i}\left(\boldsymbol{C}_i \dot{\boldsymbol{e}}_i + \boldsymbol{D}_i \boldsymbol{e}_i + \boldsymbol{g}_i + \boldsymbol{d}_i + \boldsymbol{\epsilon}_i + \boldsymbol{H}_i \boldsymbol{u}_i\right) \\ & + \sum_{j \in N_i} l_{ij} \mathbf{e}_j \end{aligned} \tag{8}$$

In order to simplify Eq. (8), define

$$\boldsymbol{z}_i \triangleq \frac{1}{m_i}\left(\boldsymbol{C}_i \dot{\boldsymbol{e}}_i + \boldsymbol{D}_i \boldsymbol{e}_i + \boldsymbol{g}_i\right) + \sum_{j \in N_i} l_{ij} \mathbf{e}_j \tag{9}$$

Then the second derivative of the global formation tracking error $\boldsymbol{\Delta}_i$ can be written as

$$\ddot{\boldsymbol{\Delta}}_i = \boldsymbol{z}_i + \frac{1}{m_i}\left(\boldsymbol{d}_i + \boldsymbol{\epsilon}_i + \boldsymbol{H}_i \boldsymbol{u}_i\right) \tag{10}$$

In order to facilitate controller design, the sum of bias fault and external disturbance $(d_{ik} + \epsilon_{ik})$ is assumed to be bounded and such that $\|d_{ik} + \epsilon_{ik}\| \leqslant Y_{ik}$, where $Y_{ik} \in \mathbb{R}^{+}$ is an unknown positive constant, $k = x, y, z$ denotes the three axes with respect to the F_C frame.

3.1. Prescribed performance control method

The PPC structure has three key steps. The first step is to design prescribed performance constraints. The second step is to deal with the performance constraint. The third step is to achieve the prescribed performance. In this subsection, the first two steps are described.

In the first step, the constraints of the controlled system should be modeled as performance boundary constraints. In the traditional performance boundary constraints, a set of inequalities is used to limit the upper and lower bounds of the state varible, which can be described as:

$$\begin{cases} -\delta\rho(t) < e(t) < \rho(t) & e(0) \geqslant 0 \\ -\rho(t) < e(t) < -\delta\rho(t) & e(0) < 0 \end{cases} \tag{11}$$

where $e(t)$ is the state varible, $\delta \in (0\,1]$ is the positive constant to be designed. The performance function is $\rho(t)$. In general, two conditions for the $\rho(t)$ need to be satisfied by

(1) $\rho(t)$ is a time-dependent and decreasing function.

(2) $\rho(t)$ should be continuous and differentiable.

In this work, a positive decreasing smooth function is chosen as the performance function, which can be expressed as

$$\rho(t) = (\rho_0 - \rho_\infty) e^{-at} + \rho_\infty \tag{12}$$

where ρ_0, ρ_∞, a are the positive constants to be designed. The initial value of $\rho(t)$ is ρ_0, which should be greater than the initial value of the state varible norm. The final value of $\rho(t)$ is ρ_∞, which can ensure that the state varible eventually converges to ρ_∞. The rate of exponential convergence is a. The execution capability of the actual system should be considered in the design.

However, inequality constraints increase challenges for the controller design. To facilitate controller design, the inequality constraints need to be transformed into equality constraints, which is the second step in the PPC structure. In this step, a standard state η is first introduced, which is denoted as

$$\eta = \frac{e(t)}{\rho(t)} \tag{13}$$

Then, a logarithmic function is introduced to transform the constrained error, the transformed error variable ε is as follows

$$\varepsilon = \mathcal{F}(\eta) = \frac{1}{2} \ln\left(\frac{1+\eta}{1-\eta}\right) \tag{14}$$

where $\mathcal{F}(\cdot)$ is the homeomorphic mapping function. Based on Eq. (14), it can be found that when the state varible is within the constraints, the transformed error variable satisfy $\varepsilon \in (-\infty, +\infty)$. This means that the transformed nonlinear system is unconstrained. Therefore, the difficulty can be reduced by using the transformed system to design the controller. Designing a controller that can guarantee ε is bounded and approaches zero in finite time becomes a new control problem.

To facilitate the design of the controller, taking the second derivative of Eq. (13) and Eq. (14) respectively, we can obtain

$$\ddot{\eta} = \frac{\ddot{e}}{\rho} - \frac{\ddot{\rho} e + 2\dot{\rho}\dot{e}}{\rho^2} + \frac{2\dot{\rho}^2 e}{\rho^3} \tag{15}$$

$$\ddot{\varepsilon} = \frac{\ddot{\eta}}{(1+\eta)(1-\eta)} + \frac{2\eta\dot{\eta}}{(1+\eta)^2(1-\eta)^2} \tag{16}$$

Substituting Eq. (15) into Eq. (16), one can obtain

$$\ddot{\varepsilon} = \frac{1}{(1+\eta)(1-\eta)}\left(\frac{\ddot{e}}{\rho} - \frac{\ddot{\rho}e + 2\dot{\rho}\dot{e}}{\rho^2} + \frac{2\dot{\rho}^2 e}{\rho^3}\right) + \frac{2\eta\dot{\eta}}{(1+\eta)^2(1-\eta)^2} \tag{17}$$

In order to simplify Eq. (17), define

$$\begin{aligned} G &\triangleq \tfrac{1}{(1+\eta)(1-\eta)\rho} \\ Q &\triangleq \tfrac{\ddot{\rho}e+2\dot{\rho}\dot{e}}{(1+\eta)(1-\eta)\rho^2} + \tfrac{2\dot{\rho}^2 e}{(1+\eta)(1-\eta)\rho^3} + \tfrac{2\eta\dot{\eta}}{(1+\eta)^2(1-\eta)^2} \end{aligned} \tag{18}$$

Based on Eq. (18), Eq. (17) can be written as

$$\ddot{\varepsilon} = G\ddot{e} + Q \tag{19}$$

Substituting Eq. (10) into Eq. (19), we can get the transformed global formation tracking error, which can be expressed as

$$\ddot{\boldsymbol{\varepsilon}}_i = \boldsymbol{G}_i\left[\boldsymbol{z}_i + \frac{1}{m_i}(\boldsymbol{d}_i + \boldsymbol{\epsilon}_i + \boldsymbol{H}_i\boldsymbol{u}_i)\right] + \boldsymbol{Q}_i \tag{20}$$

where $\varepsilon_i = \left[\varepsilon_{ix}, \varepsilon_{iy}, \varepsilon_{iz}\right]^{\mathrm{T}}$, $\boldsymbol{G}_i = \mathrm{diag}\left(G_{ix}, G_{iy}, G_{iz}\right)$, $\boldsymbol{Q}_i = \left[Q_{ix}, Q_{iy}, Q_{iz}\right]^{\mathrm{T}}$.

3.2. Controller design

In the previous subsections, prescribed performance constraints were first introduced. Then the controlled system was transformed into an unconstrained one by homeomorphic mapping.

In this subsection, the controller of the transformed nonlinear system will be designed to achieve the control goal. Since the PPC structure has no requirements for the controller, the sliding mode control with better robustness is chosen in this work. In order to avoid the singular problem of the traditional sliding mode and improve the convergence speed of the sliding mode system. The controller is designed by combining the Nonsingular Fast Terminal Sliding Mode Control with the Variable Exponential Reaching Law. Variable Exponential Reaching Law was proposed in the authors' previous work (Wu et al., 2019). The structure of Variable Exponential Reaching Law is given as

$$\dot{\boldsymbol{s}}_i = -\boldsymbol{k}_i\boldsymbol{s}_i - \boldsymbol{q}_i\tanh(\tau\boldsymbol{s}_i) \tag{21}$$

where $\boldsymbol{k}_i = \mathrm{diag}\left(k_{ix}, k_{iy}, k_{iz}\right)$, $\tanh(\tau\boldsymbol{s}_i) = [\tanh(\tau s_{ix}), \tanh\left(\tau s_{iy}\right)\tanh(\tau s_{iz})]^{\mathrm{T}}$, τ is the positive constant to be designed, $\boldsymbol{q}_i = \mathrm{diag}\left(q_{ix}, q_{iy}, q_{iz}\right)$.

Yang and Yang (2011) proposed the nonsingular fast terminal sliding mode control, and proved its characteristics of fast convergence in a limited time and avoiding singularity problems. The structure of nonsingular fast terminal sliding mode with transformed error can be expressed as

$$\boldsymbol{s}_i = \boldsymbol{\varepsilon}_i + \Lambda_1\mathrm{sign}^{\Gamma_1}\boldsymbol{\varepsilon}_i + \Lambda_2\mathrm{sign}^{\Gamma_2}\dot{\boldsymbol{\varepsilon}}_i \tag{22}$$

where $\boldsymbol{s}_i$ denotes 3-dimensional sliding surface, and the involved matrices are represented by

$$\begin{aligned} \Lambda_1 &= \mathrm{diag}(\lambda_{11}, \lambda_{12}, \lambda_{13}) \qquad \Gamma_1 = \mathrm{diag}(\gamma_{11}, \gamma_{12}, \gamma_{13}) \\ \Lambda_2 &= \mathrm{diag}(\lambda_{21}, \lambda_{22}, \lambda_{23}) \qquad \Gamma_2 = \mathrm{diag}(\gamma_{21}, \gamma_{22}, \gamma_{23}) \end{aligned} \tag{23}$$

with $\lambda_{1i} > 0, \lambda_{2i} > 0, \gamma_{1i} > \gamma_{2i}$, $1 < \gamma_{2i} < 2$, for $i = 1, 2, 3$.

The $\mathrm{sign}^{\Gamma_1}\boldsymbol{\varepsilon}_i$ is a vector defined as

$$\begin{aligned} \mathrm{sign}^{\Gamma_1}\boldsymbol{\varepsilon}_i &\triangleq [\mathrm{sign}^{\gamma_{11}}\varepsilon_{i1}, \mathrm{sign}^{\gamma_{12}}\varepsilon_{i2}, \mathrm{sign}^{\gamma_{13}}\varepsilon_{i3}]^{\mathrm{T}} \\ &= [|\varepsilon_{i1}|^{\gamma_{11}}\mathrm{sign}\,\varepsilon_{i1}, |\varepsilon_{i2}|^{\gamma_{12}}\mathrm{sign}\,\varepsilon_{i2}, |\varepsilon_{i3}|^{\gamma_{13}}\mathrm{sign}\,\varepsilon_{i3}]^{\mathrm{T}} \end{aligned} \tag{24}$$

The $\mathrm{sign}^{\Gamma_2}\dot{\boldsymbol{\varepsilon}}_i$ is a vector defined as

$$\begin{aligned} \mathrm{sign}^{\Gamma_2}\dot{\boldsymbol{\varepsilon}}_i &\triangleq [\mathrm{sign}^{\gamma_{21}}\dot{\varepsilon}_{i1}, \mathrm{sign}^{\gamma_{22}}\dot{\varepsilon}_{i2}, \mathrm{sign}^{\gamma_{23}}\dot{\varepsilon}_{i3}]^{\mathrm{T}} \\ &= [|\dot{\varepsilon}_{i1}|^{\gamma_{21}}\mathrm{sign}\,\dot{\varepsilon}_{i1}, |\dot{\varepsilon}_{i2}|^{\gamma_{22}}\mathrm{sign}\,\dot{\varepsilon}_{i2}, |\dot{\varepsilon}_{i3}|^{\gamma_{23}}\mathrm{sign}\,\dot{\varepsilon}_{i3}]^{\mathrm{T}} \end{aligned} \tag{25}$$

The time-derivatives of $\mathrm{sign}^{\Gamma_1}\boldsymbol{\varepsilon}_i$ and $\mathrm{sign}^{\Gamma_2}\dot{\boldsymbol{\varepsilon}}_i$ are given by

$$\begin{aligned} \tfrac{\mathrm{d}}{\mathrm{d}t}\left(\mathrm{sign}^{\Gamma_1}\boldsymbol{\varepsilon}_i\right) &= \Gamma_1\,\mathrm{diag}\left(|\boldsymbol{\varepsilon}_i|^{\Gamma_1-\mathrm{I}_3}\right)\dot{\boldsymbol{\varepsilon}}_i \\ \tfrac{\mathrm{d}}{\mathrm{d}t}\left(\mathrm{sign}^{\Gamma_2}\dot{\boldsymbol{\varepsilon}}_i\right) &= \Gamma_2\,\mathrm{diag}\left(|\dot{\boldsymbol{\varepsilon}}_i|^{\Gamma_2-\mathrm{I}_3}\right)\ddot{\boldsymbol{\varepsilon}}_i \end{aligned} \tag{26}$$

Based on Eq. (26), the time derivative of Eq. (22) can be given by

$$\begin{aligned} \dot{\boldsymbol{s}}_i = \dot{\boldsymbol{\varepsilon}}_i &+ \Lambda_1\Gamma_1\,\mathrm{diag}\left(|\boldsymbol{\varepsilon}_i|^{\Gamma_1-\mathrm{I}_3}\right)\dot{\boldsymbol{\varepsilon}}_i \\ &+ \Lambda_2\Gamma_2\,\mathrm{diag}\left(|\dot{\boldsymbol{\varepsilon}}_i|^{\Gamma_2-\mathrm{I}_3}\right)\ddot{\boldsymbol{\varepsilon}}_i \end{aligned} \tag{27}$$

In order to simplify Eq. (27), define

$$\boldsymbol{M}_i \triangleq \Lambda_1\Gamma_1\,\mathrm{diag}\left(|\boldsymbol{\varepsilon}_i|^{\Gamma_1-\mathrm{I}_3}\right) \qquad \boldsymbol{N}_i \triangleq \Lambda_2\Gamma_2\,\mathrm{diag}\left(|\dot{\boldsymbol{\varepsilon}}_i|^{\Gamma_2-\mathrm{I}_3}\right) \tag{28}$$

Based on Eq. (28), Eq. (27) can be written as

$$\dot{\boldsymbol{s}}_i = (\boldsymbol{I}_3 + \boldsymbol{M}_i)\dot{\boldsymbol{\varepsilon}}_i + \boldsymbol{N}_i\ddot{\boldsymbol{\varepsilon}}_i \tag{29}$$

Substituting Eq. (21) into Eq. (29), we can obtain

$$-\boldsymbol{k}_i\boldsymbol{s}_i - \boldsymbol{q}_i\tanh(\tau\boldsymbol{s}_i) = (\boldsymbol{I}_3 + \boldsymbol{M}_i)\dot{\boldsymbol{\varepsilon}}_i + \boldsymbol{N}_i\ddot{\boldsymbol{\varepsilon}}_i$$

Substituting Eq. (20) into Eq. (30), we can obtain

$$\begin{aligned} -\boldsymbol{k}_i\boldsymbol{s}_i - \boldsymbol{q}_i\tanh(\tau\boldsymbol{s}_i) &= (\boldsymbol{I}_3 + \boldsymbol{M}_i)\dot{\boldsymbol{\varepsilon}}_i \\ &+ \boldsymbol{N}_i\boldsymbol{G}_i\left[\boldsymbol{z}_i + \frac{1}{m_i}(\boldsymbol{d}_i + \boldsymbol{\epsilon}_i + \boldsymbol{H}_i\boldsymbol{u}_i)\right] + \boldsymbol{N}_i\boldsymbol{Q}_i \end{aligned} \tag{31}$$

According to the previous assumption, we know that $\|d_{ik} + \epsilon_{ik}\| \leqslant Y_{ik}\,(k = x, y, z)$, which means that the information upper bound of disturbance and fault is known. However, in practice, it is impossible to obtain such information in advance. To solve this problem, an adaptive law is proposed as

$$\dot{\widehat{\boldsymbol{Y}}}_i = \boldsymbol{\alpha}_i\widetilde{\boldsymbol{Y}}_i - \boldsymbol{\alpha}_i\boldsymbol{Y}_i \tag{32}$$

where $\boldsymbol{Y}_i = \left[Y_{ix}, Y_{iy}, Y_{iz}\right]^{\mathrm{T}}$, $Y_{ik}(k = x, y, z)$ is the upper bound of $(d_{ik} + \epsilon_{ik})$, and it is also the parameter to be estimated by the adaptive law. The estimation of $\boldsymbol{Y}_i$ is

$\widehat{\boldsymbol{Y}}_i = \left[\widehat{Y}_{ix}, \widehat{Y}_{iy}, \widehat{Y}_{iz}\right]^{\mathrm{T}}$. The estimation error is $\widetilde{\boldsymbol{Y}}_i = \boldsymbol{Y}_i - \widehat{\boldsymbol{Y}}_i$. $\boldsymbol{\alpha}_i = \mathrm{diag}(\alpha_{ix}, \alpha_{iy}, \alpha_{iz})$, where $\alpha_{ik}\,(k = x, y, z)$ is a positive constant to be designed.

Therefore, based on Eq. (31) and Eq. (32), the controller for each i-th sapcecraft is designed as

$$\begin{aligned}\boldsymbol{u}_i = &-m_i \boldsymbol{H}_i^{-1} \\ &\left\{(\boldsymbol{N}_i\boldsymbol{G}_i)^{-1}[\boldsymbol{k}_i\boldsymbol{s}_i + \boldsymbol{q}_i \tanh(\tau\boldsymbol{s}_i) + (\boldsymbol{I}_3 + \boldsymbol{M}_i)\dot{\boldsymbol{\varepsilon}}_i + \boldsymbol{N}_i\boldsymbol{Q}_i] + \boldsymbol{z}_i\right\} \\ &- \boldsymbol{H}_i^{-1}\widehat{\boldsymbol{Y}}_i\end{aligned} \tag{33}$$

3.3. Stability analysis

To prove the stability of the controller, *Lemma*1 is introduced.

Lemma 1 (Ge and Wang, 2004): Let the Lyapunov function candidate $V(x)$ be positive and continuously differentiable with a bounded initial value $V(\boldsymbol{x_0})$, and $\sigma\|\boldsymbol{x}\|^2 \leqslant V(\boldsymbol{x})$, where $\boldsymbol{x}$ is the system state, σ is the positive scalar. If the following inequality holds: $\dot{V}(\boldsymbol{x}) \leqslant -\Xi_0 V(\boldsymbol{x}) + \Xi_1$, where $\Xi_0 > 0, \Xi_1 > 0$, the $V(\boldsymbol{x})$ is bounded, and the solution of $\boldsymbol{x}$ will converge exponentially to a compact set $\boldsymbol{\Omega}_2 = \left\{x \middle| \|\boldsymbol{x}\| \leqslant \sqrt{\Xi_1/(\sigma\Xi_0)}\right\}$.

Proof: Consider the candidate Lyapunov function:

$$V_i = V_{i1} + V_{i2} = \frac{1}{2}\boldsymbol{s}_i^{\mathrm{T}}\boldsymbol{s}_i + \frac{1}{2}\widetilde{\boldsymbol{Y}}_i^{\mathrm{T}}\widetilde{\boldsymbol{Y}}_i \tag{34}$$

Taking the derivative of V_i along Eq. (34) yields

$$\dot{V}_i = \boldsymbol{s}_i^{\mathrm{T}}\dot{\boldsymbol{s}}_i - \widetilde{\boldsymbol{Y}}_i^{\mathrm{T}}\dot{\widehat{\boldsymbol{Y}}}_i \tag{35}$$

Substituting Eq. (10)Eq. (20) into Eq. (29), one can obtain

$$\dot{\boldsymbol{s}}_i = -\boldsymbol{q}_i \tanh(\tau\boldsymbol{s}_i) - \boldsymbol{k}_i\boldsymbol{s}_i + \boldsymbol{N}_i\boldsymbol{G}_i\left(\boldsymbol{d}_i + \boldsymbol{\epsilon}_i - \widehat{\boldsymbol{Y}}_i\right) \tag{36}$$

Substituting Eq. (36)Eq. (32) into Eq. (35) results in

$$\begin{aligned}\dot{V}_i &= \boldsymbol{s}_i^{\mathrm{T}}\left[-\boldsymbol{q}_i \tanh(\tau\boldsymbol{s}_i) - \boldsymbol{k}_i\boldsymbol{s}_i + \boldsymbol{N}_i\boldsymbol{G}_i\left(\boldsymbol{d}_i + \boldsymbol{\epsilon}_i - \widehat{\boldsymbol{Y}}_i\right)\right] \\ &\quad - \widetilde{\boldsymbol{Y}}_i^{\mathrm{T}}\left[\alpha_i\widetilde{\boldsymbol{Y}}_i - \boldsymbol{\alpha}_i\boldsymbol{Y}_i\right] \\ &= -\boldsymbol{s}_i^{\mathrm{T}}\boldsymbol{q}_i \tanh(\tau\boldsymbol{s}_i) - \boldsymbol{s}_i^{\mathrm{T}}\boldsymbol{k}_i\boldsymbol{s}_i + \boldsymbol{s}_i^{\mathrm{T}}\boldsymbol{N}_i\boldsymbol{G}_i\left(\boldsymbol{d}_i + \boldsymbol{\epsilon}_i - \widehat{\boldsymbol{Y}}_i\right) \\ &\quad - \widetilde{\boldsymbol{Y}}_i^{\mathrm{T}}\boldsymbol{\alpha}_i\widetilde{\boldsymbol{Y}}_i + \widetilde{\boldsymbol{Y}}_i^{\mathrm{T}}\boldsymbol{\alpha}_i\boldsymbol{Y}_i\end{aligned} \tag{37}$$

Based on previous assumption, we know that $(d_{ik} + \epsilon_{ik}) \leqslant Y_{ik}\,(k = x, y, z)$, so the derivative of V_i satisfies the following inequality

$$\begin{aligned}\dot{V}_i &\leqslant -\boldsymbol{s}_i^{\mathrm{T}}\boldsymbol{q}_i \tanh(\tau\boldsymbol{s}_i) - \boldsymbol{s}_i^{\mathrm{T}}\boldsymbol{k}_i\boldsymbol{s}_i + \boldsymbol{s}_i^{\mathrm{T}}\boldsymbol{N}_i\boldsymbol{G}_i\left(\boldsymbol{Y}_i - \widehat{\boldsymbol{Y}}_i\right) \\ &\quad - \widetilde{\boldsymbol{Y}}_i^{\mathrm{T}}\boldsymbol{\alpha}_i\widetilde{\boldsymbol{Y}}_i + \widetilde{\boldsymbol{Y}}_i^{\mathrm{T}}\boldsymbol{\alpha}_i\boldsymbol{Y}_i \\ &\leqslant -\boldsymbol{s}_i^{\mathrm{T}}\boldsymbol{q}_i\tau\boldsymbol{s}_i - \boldsymbol{s}_i^{\mathrm{T}}\boldsymbol{k}_i\boldsymbol{s}_i - \widetilde{\boldsymbol{Y}}_i^{\mathrm{T}}\boldsymbol{\alpha}_i\widetilde{\boldsymbol{Y}}_i + \boldsymbol{s}_i^{\mathrm{T}}\boldsymbol{N}_i\boldsymbol{G}_i\widetilde{\boldsymbol{Y}}_i + \widetilde{\boldsymbol{Y}}_i^{\mathrm{T}}\boldsymbol{\alpha}_i\boldsymbol{Y}_i \\ &= -\boldsymbol{s}_i^{\mathrm{T}}\boldsymbol{r}_i\boldsymbol{s}_i - \widetilde{\boldsymbol{Y}}_i^{\mathrm{T}}\boldsymbol{\alpha}_i\widetilde{\boldsymbol{Y}}_i + \boldsymbol{s}_i^{\mathrm{T}}\boldsymbol{N}_i\boldsymbol{G}_i\widetilde{\boldsymbol{Y}}_i + \widetilde{\boldsymbol{Y}}_i^{\mathrm{T}}\boldsymbol{\alpha}_i\boldsymbol{Y}_i\end{aligned} \tag{38}$$

where $\boldsymbol{r}_i = \boldsymbol{q}_i\tau + \boldsymbol{k}_i \in \mathbb{R}^{3\times3}$. By using the Young's inequality, after some algebraic manipulations, Eq. (38) becomes

$$\begin{aligned}&\dot{V}_i \leqslant -\boldsymbol{s}_i^{\mathrm{T}}\underline{\sigma}(r_i)\boldsymbol{I}_3\boldsymbol{s}_i - \widetilde{\boldsymbol{Y}}_i^{\mathrm{T}}\underline{\sigma}(\alpha_i)\boldsymbol{I}_3\boldsymbol{Y}_i + \tfrac{1}{2}\boldsymbol{s}_i^{\mathrm{T}}\overline{\sigma}(N_iG_i)\boldsymbol{I}_3\boldsymbol{s}_i \\ &+\tfrac{1}{2}\widetilde{\boldsymbol{Y}}_i^{\mathrm{T}}\overline{\sigma}(N_iG_i)\boldsymbol{I}_3\widetilde{\boldsymbol{Y}}_i + \tfrac{1}{2}\widetilde{\boldsymbol{Y}}_i^{\mathrm{T}}\overline{\sigma}(\alpha_i)\boldsymbol{I}_3\widetilde{\boldsymbol{Y}}_i + \tfrac{1}{2}\boldsymbol{Y}_i^{\mathrm{T}}\overline{\sigma}(\alpha_i)\boldsymbol{I}_3\boldsymbol{Y}_i \\ &= -\underline{\sigma}(r_i)\boldsymbol{s}_i^{\mathrm{T}}\boldsymbol{s}_i - \underline{\sigma}(\alpha_i)\widetilde{\boldsymbol{Y}}_i^{\mathrm{T}}\boldsymbol{Y}_i + \tfrac{1}{2}\overline{\sigma}(N_iG_i)\boldsymbol{s}_i^{\mathrm{T}}\boldsymbol{s}_i \\ &\quad +\tfrac{1}{2}\overline{\sigma}(N_iG_i)\widetilde{\boldsymbol{Y}}_i^{\mathrm{T}}\widetilde{\boldsymbol{Y}}_i + \tfrac{1}{2}\overline{\sigma}(\alpha_i)\widetilde{\boldsymbol{Y}}_i^{\mathrm{T}}\widetilde{\boldsymbol{Y}}_i + \tfrac{1}{2}\overline{\sigma}(\alpha_i)\boldsymbol{Y}_i^{\mathrm{T}}\boldsymbol{Y}_i \\ &= -[2\underline{\sigma}(r_i) - \overline{\sigma}(N_iG_i)]\tfrac{1}{2}\boldsymbol{s}_i^{\mathrm{T}}\boldsymbol{s}_i - [2\underline{\sigma}(\alpha_i) - \overline{\sigma}(N_iG_i) - \overline{\sigma}(\alpha_i)]\tfrac{1}{2} \\ &\quad \widetilde{\boldsymbol{Y}}_i^{\mathrm{T}}\widetilde{\boldsymbol{Y}}_i + \tfrac{1}{2}\overline{\sigma}(\alpha_i)\boldsymbol{Y}_i^{\mathrm{T}}\boldsymbol{Y}_i \\ &= -[2\underline{\sigma}(r_i) - \overline{\sigma}(N_iG_i)]V_{i1} - [2\underline{\sigma}(\alpha_i) - \overline{\sigma}(N_iG_i) - \overline{\sigma}(\alpha_i)]V_{i2} \\ &\quad +\tfrac{1}{2}\overline{\sigma}(\alpha_i)\boldsymbol{Y}_i^{\mathrm{T}}\boldsymbol{Y}_i \\ &= -\left[2\underline{\sigma}(r_i) - \overline{\sigma}(N_iG_i)\;2\underline{\sigma}(\alpha_i) - \overline{\sigma}(N_iG_i) - \overline{\sigma}(\alpha_i)\right]\begin{bmatrix}V_{i1}\\V_{i2}\end{bmatrix} \\ &\quad +\tfrac{1}{2}\overline{\sigma}(\alpha_i)\boldsymbol{Y}_i^{\mathrm{T}}\boldsymbol{Y}_i\end{aligned} \tag{39}$$

where $\underline{\sigma}(r_i)$ is the minimum eigenvalue of matrix $\boldsymbol{r}_i$. The minimum eigenvalue of matrix $\boldsymbol{\alpha}_i$ is $\underline{\sigma}(\alpha_i)$. The maximum eigenvalue of matrix is $\boldsymbol{\alpha}_i$ is $\overline{\sigma}(\alpha_i)$. The maximum eigenvalue of matrix $\boldsymbol{N}_i\boldsymbol{G}_i$ is $\overline{\sigma}(N_iG_i)$.

Then Eq. (39) can be reduced to

$$\begin{aligned}\dot{V}_i \leqslant &-[2\underline{\sigma}(r_i) - \overline{\sigma}(N_iG_i)2\underline{\sigma}(\alpha_i) - \overline{\sigma}(N_iG_i) - \overline{\sigma}(\alpha_i)]V_i \\ &+\tfrac{1}{2}\overline{\sigma}(\alpha_i)\boldsymbol{Y}_i^{\mathrm{T}}\boldsymbol{Y}_i\end{aligned} \tag{40}$$

Therefore, if the design constants satisfy $2\underline{\sigma}(r_i) > \overline{\sigma}(N_iG_i)$, $2\underline{\sigma}(\alpha_i) - \overline{\sigma}(\alpha_i) > \overline{\sigma}(N_iG_i)$, one can obtain

$$\dot{V}_i \leqslant -\Xi_0 V_i + \Xi_1 \tag{41}$$

implying that the system is UUB stable, see ***Lemma 1***.

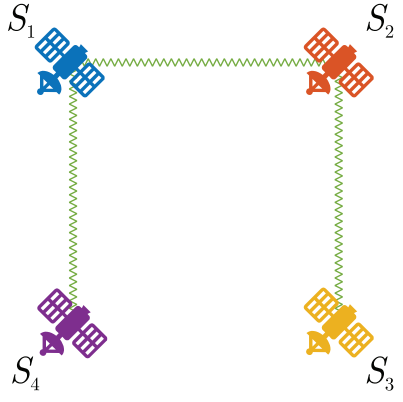

Fig. 2. Undirected communication topology among spacecraft.

Table 1
Initial simulation parameters setting.

	Values
Initial positions	$\boldsymbol{p}_1 = [33, -62, -15]^{\mathrm{T}}$ m $\quad \boldsymbol{p}_2 = [-1, -25, -14]^{\mathrm{T}}$ m $\quad \boldsymbol{p}_3 = [27, 0, 44]^{\mathrm{T}}$ m $\quad \boldsymbol{p}_4 = [-50, 32, 51]^{\mathrm{T}}$ m
Initial velocities	$\boldsymbol{v}_i = [0, 0, 0]^{\mathrm{T}}$ m/s $\quad \forall i = 1, 2, 3, 4$
Desired positions	$\boldsymbol{p}_{1d} = [0, -20\sqrt{2}, 20]^{\mathrm{T}}$ m $\quad \boldsymbol{p}_{2d} = [20\sqrt{2}, 0, 20]^{\mathrm{T}}$m $\quad \boldsymbol{p}_{3d} = [0, 20\sqrt{2}, 20]^{\mathrm{T}}$m $\quad \boldsymbol{p}_{4d} = [-20\sqrt{2}, 0, 20]^{\mathrm{T}}$m
Desired velocities	$\boldsymbol{v}_{id} = [0, 0, 0]^{\mathrm{T}}$m/s $\quad \forall i = 1, 2, 3, 4$

4. Numerical simulation

In this section, numerical simulation performed on the SFF system with actuator faults and external disturbances will test the effectiveness of the proposed method.

4.1. Initial conditions and control parameters

A SFF scenario consists of a virtual reference spacecraft and four follower spacecraft (i.e. $N = 4$). In this scenario, the spacecraft is supposed to perform a formation reconfiguration mission, changing from arbitrary four positions to a rectangular configuration in space. The undirected communication topology among spacecraft in this SFF scenario is given in Fig. 2.

The corresponding Laplacian matrix of the SFF system can be expressed as

$$\mathcal{L} = \begin{bmatrix} 2 & -1 & 0 & -1 \\ -1 & 2 & -1 & 0 \\ 0 & -1 & 1 & 0 \\ -1 & 0 & 0 & 1 \end{bmatrix} \tag{42}$$

Suppose the virtual reference spacecraft moves in an ideal elliptical orbit. The orbit parameters are set as follows: $a_c = 7178$ km, $e_c = 0.01, \Omega_c = 0$ rad, $i_c = \pi/6$, $\omega_c = 0$ rad, $\theta_c = 0$ rad. The gravitational constant is $\mu = 3.986 \times 10^{14}\mathrm{m}^3/\mathrm{s}^2$. The mass of each i-th spacecraft is $m_i = 150$ kg. The optional parameters and the initial conditions are listed in Table 1.

Suppose the actuators of each spacecraft can only provide 70% of the required control input, so the health indicator matrix can be expressed as $\boldsymbol{H}_i = 0.7\boldsymbol{I}_3$. Meanwhile, suppose the actuator bias fault $\boldsymbol{\epsilon}_i$ fluctuates randomly in a small cubic space, i.e. $\left\{\boldsymbol{\epsilon}_i \mid \boldsymbol{\epsilon}_i \in \left[10^{-3}, 10^{-3}\right]^2 \text{ deg} \times \left[10^{-2}, 10^{-2}\right]\right\}$. The external disturbances of each spacecraft are as follows

$$\boldsymbol{d}_i = \begin{bmatrix} -5 + 4\sin(0.5t + 7) + \sin\left(\frac{\pi}{2} + 0.1t\right) \\ 3 + 6\sin(t + 5) + \sin\left(\frac{\pi}{4} + 0.5t\right) \\ 8 + 2\sin(0.5t + 0.6) + \sin\left(\frac{\pi}{4} + t\right) \end{bmatrix} \times 10^{-4}\,\mathrm{N} \tag{43}$$

The parameters of the controllers are listed in Table 2.

4.2. Simulation results

This subsection presents the numerical simulation results of the proposed controller for SFF reconfiguration with actuator faults and external disturbances.

Fig. 3. shows the trajectory of each spacecraft in 3D space. We can infer from it that each trajectory is smooth,

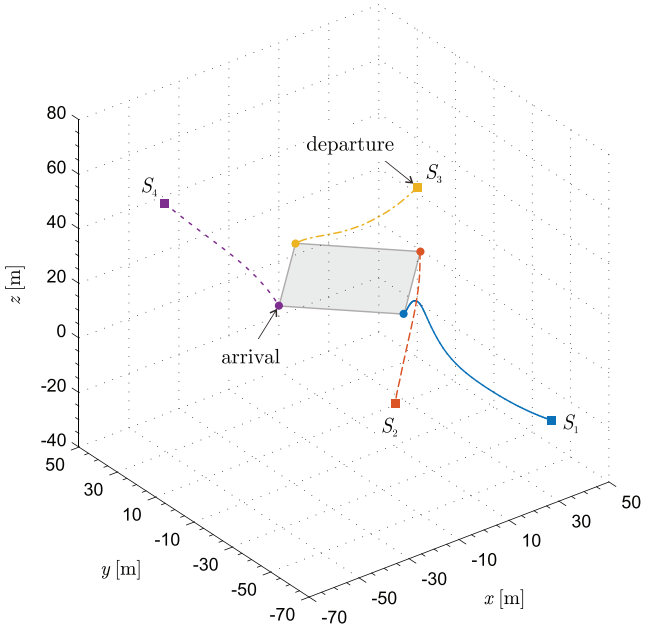

Fig. 3. 3D trajectory.

Table 2
Controller parameters setting for simulation.

Values
$\rho_0 = 80 \quad \rho_\infty = 10^{-5} \quad a = 8.5 \times 10^{-4} \quad \boldsymbol{\alpha} = 10^{-2}\boldsymbol{I}_3 \quad \widehat{\boldsymbol{Y}}(0) = 10^{-4}\boldsymbol{I}_3$
$\Lambda_1 = 10\boldsymbol{I}_3 \quad \Lambda_2 = 5\boldsymbol{I}_3 \quad \Gamma_1 = 8\boldsymbol{I}_3 \quad \Gamma_2 = 1.2\boldsymbol{I}_3 \quad \boldsymbol{k}_i = 10^{-2}\boldsymbol{I}_3 \quad \boldsymbol{q}_i = 10^{-3}\boldsymbol{I}_3 \quad \tau = 1000$

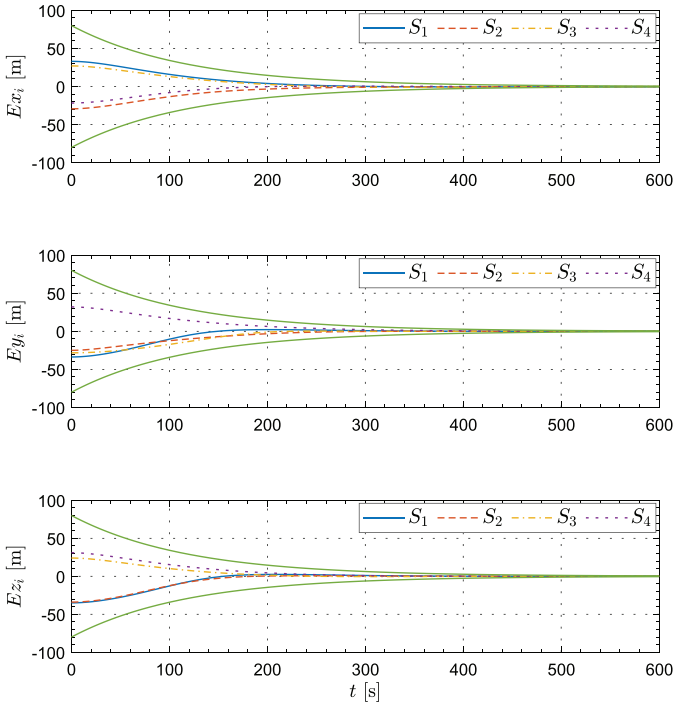

Fig. 4. Time history of formation tracking error.

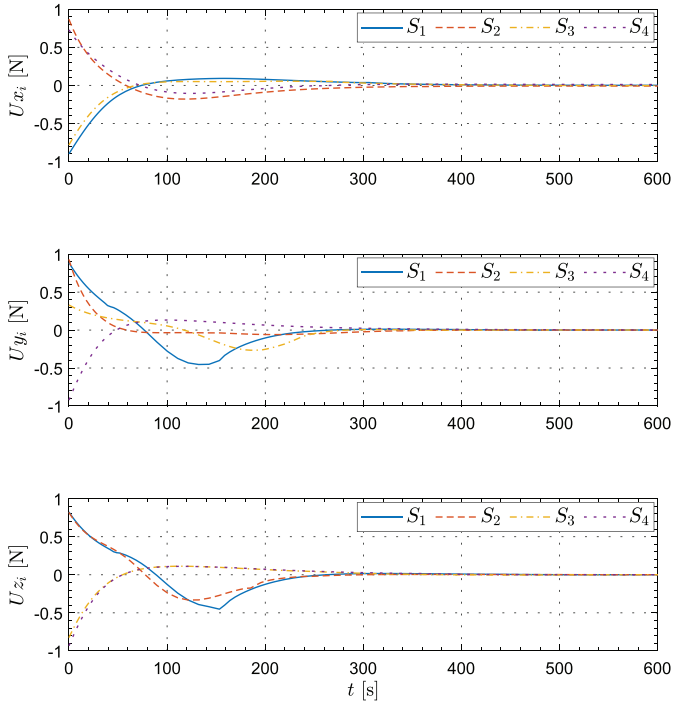

Fig. 5. Time history of control input.

and four spacecraft finally form the desired square configuration.

Fig. 4. presents the formation tracking error among each spacecraft. It can be seen that the tracking error of each spacecraft evolve smoothly within the convergence range specified by PPC, and converge to the tiny neighborhood around the origin. Fig.5. and Fig.6. depict the control input and relative velocity of each spacecraft, respectively. From these two figures, despite faults, external disturbances and uncertainties, we can see that the controller not only avoids chattering and singularity, but also reaches the target velocity in 380 s, which indicates that the proposed controller has strong robustness and fast convergence.

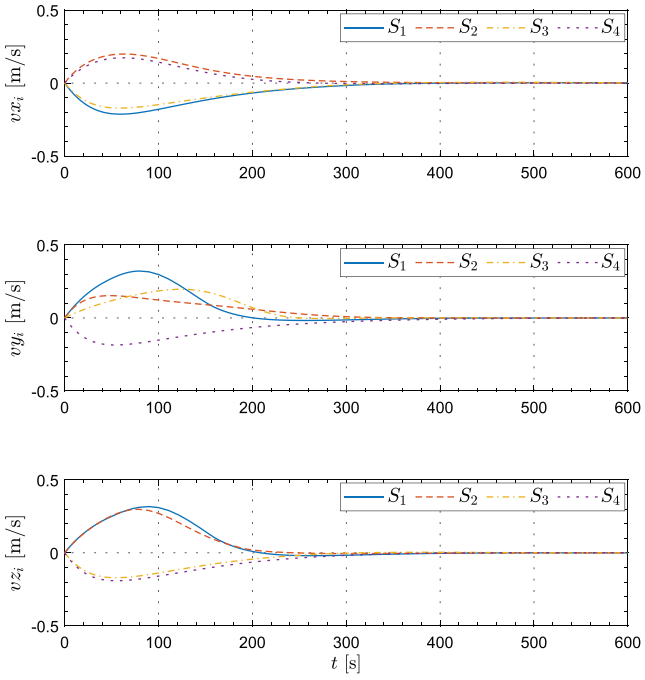

Fig. 6. Time history of relative velocity.

5. Conclusions

In this paper, the problem of adaptive fault-tolerant control for the SFF reconfiguration with prescribed performance constraints, unknown inertial uncertainties and external disturbances has been studied.First, the SFF orbit model including actuator faults is established by introducing fault factors, which can better reflect real space missions. Then, based on the PPC structure and nonsingular fast terminal sliding mode control, through incorporating the adaptive strategy, an adaptive fault-tolerant controller is proposed. Finally, the simulation indicates that the proposed algorithm is not only effective against actuator faults and external disturbances, but also speeds up convergence. Obstacle avoidance and communication maintenance are not considered due to the limitation of paper length. We will consider the elements in future work.

Declaration of Competing Interest

The authors declare that they have no known competing financial interests or personal relationships that could have appeared to influence the work reported in this paper.

Acknowledgement

This work was supported by the National Key Research and Development Program of China (Grant No. 2022YFC2204800), the National Natural Science Foundation of China (Grant Nos. 12272223 and U20B2056), and Natural Science Foundation of Shanghai (Grant No. 23ZR1433600).

References

Amaro-Seoane, P., Audley, H., Babak, S., Baker, J., Barausse, E., Bender, P., Berti, E., Binetruy, P., Born, M., Bortoluzzi, D., et al., 2017. Laser interferometer space antenna. Tp.umu.se 548, 411.

Artitthang, P., Xu, M., Lin, M., He, Y., 2023. Robust optimal sliding mode control for the deployment of coulomb spacecraft formation flying. Adv. Space Res. 71, 439–455.

Bai, Y., Biggs, J.D., Zazzera, F.B., Cui, N., 2018. Adaptive attitude tracking with active uncertainty rejection. J. Guidance Control Dyn. 41, 550–558.

Bechlioulis, C.P., Rovithakis, G.A., 2008. Robust adaptive control of feedback linearizable MIMO nonlinear systems with prescribed performance. IEEE Trans. Autom. Control 53, 2090–2099.

Cao, T., Gong, H., Cheng, P., Xue, Y., 2022. A novel learning observer-based fault-tolerant attitude control for rigid spacecraft. Aerosp. Sci. Technol. 128, 107751.

Clark, S., 2016. Attitude control failures led to break-up of japanese astronomy satellite. Spaceflight Now, pp. 140–146.

Di, F., Li, A., Guo, Y., Xie, C., Wang, C., 2021. Event-triggered sliding mode attitude coordinated control for spacecraft formation flying system with disturbances. Acta Astronaut. 188, 121–129.

Di Mauro, G., Lawn, M., Bevilacqua, R., 2018. Survey on guidance navigation and control requirements for spacecraft formation-flying missions. J. Guidance Control Dyn. 41, 581–602.

Fraser, C.T., Ulrich, S., 2021. Adaptive extended kalman filtering strategies for spacecraft formation relative navigation. Acta Astronaut. 178, 700–721.

Ge, S., Wang, C., 2004. Adaptive neural control of uncertain mimo nonlinear systems. IEEE Trans. Neural Networks 15, 674–692.

Gong, Y., Luo, J., Wang, B., 2021. Concepts and status of chinese space gravitational wave detection projects. Nat. Astron. 5, 881–889.

Guo, Y., Huang, B., Song, S., Li, A., Wang, C., 2019. Robust saturated finite-time attitude control for spacecraft using integral sliding mode. J. Guidance Control Dyn. 42, 440–446.

Han, Y., Biggs, J.D., Cui, N., 2015. Adaptive fault-tolerant control of spacecraft attitude dynamics with actuator failures. J. Guidance Control Dyn. 38, 2033–2042.

Harland, D.M., Lorenz, R.D., 2005. Attitude control system failures. Space Systems Failures: Disasters and Rescues of Satellites, Rockets and Space Probes, pp. 211–226.

Hasan, M.N., Haris, M., Qin, S., 2022. Fault-tolerant spacecraft attitude control: A critical assessment. Prog. Aerosp. Sci. 130, 100806.

Hu, Q., 2008. Sliding mode maneuvering control and active vibration damping of three-axis stabilized flexible spacecraft with actuator dynamics. Nonlinear Dyn. 52, 227–248.

Hu, Q., Xiao, L., Wang, C., 2019. Adaptive fault-tolerant attitude tracking control for spacecraft with time-varying inertia uncertainties. Chin. J. Aeronaut. 32, 674–687.

Hu, W., Wu, Y., 2017. Taiji program in space for gravitational wave physics and nature of gravity. Nat. Sci. Rev. 4, 2.

Ji, X., Li, Y., Liu, G., Wang, J., Xiang, S., Yang, X., Bi, Y., 2019. A brief review of ground and flight failures of chinese spacecraft. Prog. Aerosp. Sci. 107, 19–29.

Li, X., Luo, X., Wang, J., Guan, X., 2018. Finite-time consensus of nonlinear multi-agent system with prescribed performance. Nonlinear Dyn. 91, 2397–2409.

Lian, Y., Huo, Z., Cheng, Y., 2021. On the dynamics and control of the sun—earth l2 tetrahedral formation. Astrodynamics 5, 331–346.

Liu, C., Ye, D., Shi, K., Sun, Z., 2017. Robust high-precision attitude control for flexible spacecraft with improved mixed h2/h? control strategy under poles assignment constraint. Acta Astronaut. 136, 166–175.

Liu, G., Zhang, S., 2018. A survey on formation control of small satellites. Proc. IEEE, 106, 440–457.

Liu, Z., Yue, C., Wu, F., Wang, F., Cao, X., 2023. Data-driven prescribed performance control for satellite with large rotational component. Adv. Space Res. 71, 744–755.

Lu, K., Xia, Y., 2013. Adaptive attitude tracking control for rigid spacecraft with finite-time convergence. Automatica 49, 3591–3599.

Luo, J., Chen, L., Duan, H., Gong, Y., Hu, S., Ji, J., Liu, Q., Mei, J., Milyukov, V., Sazhin, M., et al., 2016. Tianqin: a space-borne gravitational wave detector. Class. Quantum Gravity 33, 035010.

Luo, W., Chu, Y., Ling, K., 2005. H-infinity inverse optimal attitude-tracking control of rigid spacecraft. J. Guidance Control Dyn. 28, 481–494.

Mehdifar, F., Bechlioulis, C.P., Hashemzadeh, F., Baradarannia, M., 2020. Prescribed performance distance-based formation control of multi-agent systems. Automatica 119, 109086.

Tan, C., Hu, T., Wang, D., Liu, Y., Jiang, D., Shi, J., 2011. Analysis on foreign spacecraft in-orbit failures. Spacecraft Eng. 20, 130–136.

Wang, K., Meng, T., Wang, W., Song, R., Jin, Z., 2022. Finite-time extended state observer based prescribed performance fault tolerance control for spacecraft proximity operations. Adv. Space Res. 70, 1270–1284.

Wang, W., Mengali, G., Quarta, A.A., Baoyin, H., 2020. Decentralized fault-tolerant control for multiple electric sail relative motion at artificial lagrange points. Aerosp. Sci. Technol. 103, 105904.

Wang, W., Mengali, G., Quarta, A.A., Yuan, J., 2017. Formation flying for electric sails in displaced orbits. part ii: distributed coordinated control. Adv. Space Res. 60, 1130–1147.

Wang, X., Tan, C., Wu, F., Wang, J., 2021. Fault-tolerant attitude control for rigid spacecraft without angular velocity measurements. IEEE Trans. Cybernet. 51, 1216–1229.

Wei, C., Chen, Q., Liu, J., Yin, Z., Luo, J., 2021. An overview of prescribed performance control and its application to spacecraft attitude system. Proc. Inst. Mech. Eng., Part I: J. Syst. Control Eng. 235, 435–447.

Wei, C., Wu, X., Xiao, B., Wu, J., Zhang, C., 2022. Adaptive leader-following performance guaranteed formation control for multiple spacecraft with collision avoidance and connectivity assurance. Aerosp. Sci. Technol. 120, 107266.

Wen, T., Zeng, X., Circi, C., Gao, Y., 2020. Hop reachable domain on irregularly shaped asteroids. J. Guidance Control Dyn. 43, 1269–1283.

Wu, Y., Wu, S., Gong, D., Kang, Z., Wang, X., 2019. Spacecraft attitude maneuver using fast terminal sliding mode control based on variable exponential reaching law. Int. Conf. Aerospace Syst. Sci. Eng. 622, 1–10.

Xie, X., Jiang, F., Li, J., 2023. Design and optimization of stable initial heliocentric formation on the example of lisa. Adv. Space Res. 71, 420–438.

Yang, L., Yang, J., 2011. Nonsingular fast terminal sliding-mode control for nonlinear dynamical systems. Int. J. Robust Nonlinear Control 21, 1865–1879.

Yi, H., Liu, M., Li, M., 2019. Event-triggered fault tolerant control for spacecraft formation attitude synchronization with limited data communication. Eur. J. Control 48, 97–103.

Yin, S., Xiao, B., Ding, S.X., Zhou, D., 2016. A review on recent development of spacecraft attitude fault tolerant control system. IEEE Trans. Industr. Electron. 63, 3311–3320.

Yin, T., Zhang, K., Jiang, B., Liu, Q., 2022. Fixed-time attitude cooperative fault-tolerant control with prescribed performance for heterogeneous multiple satellite. Aerosp. Sci. Technol. 128, 107752.

Yue, C., Wang, F., Cao, X., Shen, Q., Chen, X., 2020. Robust fault-tolerant attitude tracking with guaranteed prescribed performance. J. Franklin Inst. 357, 229–253.
Zhang, B., Li, F., 2022. Adaptive finite-time control for six-degree-of-freedom leader-following spacecraft formation using twistors. Adv. Space Res. 70, 1297–1311.
Zhang, C., Dai, M., Wu, J., Xiao, B., Li, B., Wang, M., 2021. Neural-networks and event-based fault-tolerant control for spacecraft attitude stabilization. Aerosp. Sci. Technol. 114, 106746.
Zhang, C., Wang, J., Zhang, D., Shao, X., 2018. Fault-tolerant adaptive finite-time attitude synchronization and tracking control for multi-spacecraft formation. Aerosp. Sci. Technol. 73, 197–209.
Zhang, J., Zhao, W., Shen, G., Xia, Y., 2020. Disturbance observer-based adaptive finite-time attitude tracking control for rigid spacecraft. IEEE Trans. Syst. Man Cybernet.: Syst. 51, 6606–6613.
Zhu, W., Zong, Q., Tian, B., Liu, W., 2020. Disturbance observer-based active vibration suppression and attitude control for flexible spacecraft. IEEE Trans. Syst. Man Cybernet.: Syst. 52, 893–901.
Zhu, Z., Guo, Y., 2018. Adaptive fault-tolerant attitude tracking control for spacecraft formation with unknown inertia. Int. J. Adapt. Control Signal Process. 32, 13–26.
Zhuang, M., Tan, L., Li, K., Song, S., 2021a. Fixed-time formation control for spacecraft with prescribed performance guarantee under input saturation. Aerosp. Sci. Technol. 119, 107176.
Zhuang, M., Tan, L., Li, K., Song, S., 2021b. Fixed-time position coordinated tracking control for spacecraft formation flying with collision avoidance. Chin. J. Aeronaut. 34, 182–199.